Atmospheric
Chemistry
and Physics

Changes in biomass burning, wetland extent, or agriculture drive atmospheric NH₃ trends in select African regions

Jonathan E. Hickman[1], Niels Andela[2,a], Enrico Dammers[3], Lieven Clarisse[4], Pierre-François Coheur[4],
Martin Van Damme[4], Courtney A. Di Vittorio[5], Money Ossohou[6,b], Corinne Galy-Lacaux[7], Kostas Tsigaridis[1,8], and
Susanne E. Bauer[1]

[1]NASA Goddard Institute for Space Studies, New York, USA
[2]NASA Goddard Space Flight Center, Greenbelt, USA
[3]Climate Air and Sustainability, Netherlands Organisation for Applied Scientific Research (TNO), Utrecht, the Netherlands
[4]Atmospheric Spectroscopy, Service de Chimie Quantique et Photophysique, Université libre de Bruxelles (ULB), Brussels,
Belgium
[5]Department of Engineering, Wake Forest University, Winston-Salem, USA
[6]Laboratoire des Sciences de la Matière, de l'Environnement et de l'Energie Solaire,
Université Félix Houphouët-Boigny, Abidjan, Côte d'Ivoire
[7]Laboratoire d'Aérologie, Université Toulouse III Paul Sabatier / CNRS, Toulouse, France
[8]Center for Climate Systems Research, Columbia University, New York, USA
[a]now at: School of Earth and Environmental Sciences, Cardiff University, Cardiff, UK
[b]now at: Sciences technologie, University of Man, Man, Côte d'Ivoire

Correspondence: Jonathan E. Hickman (jonathan.e.hickman@nasa.gov)

Abstract. TS1 Atmospheric ammonia (NH₃) is a precursor to fine particulate matter and a source of nitrogen (N) deposition that can adversely affect ecosystem health. The main sources of NH₃ – agriculture and biomass burning – are undergoing are or expected to undergo substantial changes in Africa. Although evidence of increasing NH₃ over parts of Africa has been observed, the mechanisms behind these trends are not well understood. Here we use observations of atmospheric NH₃ vertical column densities (VCDs) from the Infrared Atmospheric Sounding Interferometer (IASI) along with other satellite observations of the land surface and atmosphere to evaluate how NH₃ concentrations have changed over Africa from 2008 through 2018, and what has caused those changes. In West Africa NH₃ VCDs are observed to increase during the late dry season, with increases of over 6 % yr⁻¹ in Nigeria during February and March ($p < 0.01$). These positive trends are associated with increasing burned area and CO trends during these months, likely related to agricultural preparation. Increases are also observed in the Lake Victoria basin region, where they are associated with expanding agricultural area. In contrast, NH₃ VCDs declined over the Sudd wetlands in South Sudan by over 1.5 % yr⁻¹, though not significantly ($p = 0.28$). Annual maxima in NH₃ VCDs in South Sudan occur during February through May and are associated with the drying of temporarily flooded wetland soils, which favor emissions of NH₃. The change in mean NH₃ VCDs over the Sudd is strongly correlated with variation in wetland extent in the Sudd: in years when more area remained flooded during the dry season, NH₃ VCDs were lower ($r = 0.64$, $p < 0.05$). Relationships between biomass burning and NH₃ may be observed when evaluating national-scale statistics: countries with the highest rates of increasing NH₃ VCDs also had high rates of growth in CO VCDs; burned area displayed a similar pattern, though not significantly. Livestock numbers were also higher in countries with intermediate or high rates of NH₃ VCD growth. Fertilizer use in Africa is currently low but growing; implementing practices that can limit NH₃ losses from fertilizer as agriculture is intensified may help mitigate impacts on health and ecosystems.

1 Introduction

Ammonia (NH_3), a reactive nitrogen (N) trace gas, plays a number of important roles in the atmosphere, with implications for human health, climate, and ecosystems. Once in the atmosphere, NH_3 contributes to the production of inorganic aerosols, the primary constituents of fine particulate matter and a serious health hazard (Bauer et al., 2016; Lelieveld et al., 2015; Pope et al., 2002). NH_3 can also be deposited to downwind ecosystems, contributing to eutrophication, soil acidification, vegetation damage, productivity declines, reductions in biodiversity, and indirect greenhouse gas emissions (Denier Van Der Gon and Bleeker, 2005; Krupa, 2003; Matson et al., 1999; Stevens et al., 2018; Tian and Niu, 2015).

Although NH_3 is emitted from natural soils, agriculture is by far the largest source of NH_3 globally (Behera et al., 2013; Bouwman et al., 1997). Urea fertilizer and livestock excreta are particularly important substrates for NH_3 formation and can be volatilized quickly under favorable environmental conditions (Bouwman et al., 1997). In all soils, NH_3 is formed in solution following the dissociation of ammonium (NH_4^+; Eq. 1).

$$NH_4^+ + OH^- \leftrightarrow H_2O + NH_3 \tag{1}$$
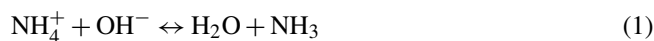
Soil NH_3 production is temperature-dependent, doubling with every $5\,°C$ temperature increase, though the actual soil NH_3 flux is determined in part by plant and soil physiological and physical factors (Sutton et al., 2013). On average, fertilizer use has been extremely low in sub-Saharan Africa – often an order of magnitude or more lower than typical in Europe, the United States, or China (Hazell and Wood, 2008; Vitousek et al., 2009). Livestock manure N content also tends to be very low in sub-Saharan Africa (Rufino et al., 2006). The low fertilizer use suggests that natural soils (as opposed to agricultural soils) may be a more important source in the region than elsewhere in the world. However, agricultural intensification and increasing fertilizer use has been a central policy focus for many African countries, with national and regional efforts to increase N inputs by an order of magnitude or more (AGRA, 2009).

After agriculture, biomass burning is the most important source of NH_3 globally (Bouwman et al., 1997), with roughly 60 % to 70 % of global NH_3 emissions from fires occurring in Africa (Cahoon et al., 1992; Whitburn et al., 2015). The amount of NH_3 emitted from biomass fires is controlled primarily by the type of burning that occurs. N in fuel is present predominantly in a chemically reduced state, and NH_3 is emitted in greater quantities from low-temperature smoldering combustion in which fuel N is incompletely oxidized (Goode et al., 1999; Yokelson et al., 2008). Fuel moisture content, which can help determine whether combustion is smoldering or flaming, is thus an important determinant of biomass burning NH_3 emissions (Chen et al., 2010).

In contrast to other reactive N gases such as NO_x (nitric oxide + nitrogen dioxide), NH_3 emissions are typically unregulated outside of Europe (Anker et al., 2018; Kanter, 2018; USDA Agricultural Air Quality Task Force, 2014), and substantial increasing trends have been observed by the NASA Atmospheric InfraRed Sounder (AIRS) and the Infrared Atmospheric Sounding Interferometer (IASI) over many of the world's major agricultural and biomass burning regions during the 21st century (Van Damme et al., 2021; Warner et al., 2017). West Africa has been identified as an important NH_3 source region (Van Damme et al., 2018), where a trend of increasing NH_3 concentrations in recent decades has been attributed at least in part to increased fertilizer use (Van Damme et al., 2021; Warner et al., 2017). Increasing trends have also been observed over central Africa and have been attributed to higher rates of biomass burning (Van Damme et al., 2021; Warner et al., 2017). However, the studies by Warner et al. (2017) and Van Damme et al. (2021) were global in nature, and as such could not include detailed explorations of the drivers of trends such as consideration of emission seasonality or the geographic distribution of emission drivers. Consideration of these factors is particularly important across large parts of Africa where both biomass burning and soils are potentially important sources of NH_3 (van der A et al., 2008).

Here we use an 11-year satellite record to evaluate trends in atmospheric NH_3 concentrations over Africa from 2008 through 2018, including a detailed examination of three regions where changes are pronounced: West Africa, the Lake Victoria basin region, and South Sudan.

2 Data and methods

2.1 Global gridded data

Multiple data products were used, including satellite observations and spatial datasets:

- IASI-A, launched aboard the European Space Agency's MetOp-A in 2006, provides measurements of atmospheric NH_3 and carbon monoxide (CO) twice a day (9:30 in the morning and 21:30 in the evening, Local Solar Time at the Equator). Here we use morning observations, when the thermal contrast is more favorable for retrievals (Clarisse et al., 2009; Van Damme et al., 2014a). The NH_3 retrieval product used (ANNI-NH3-v3R) follows a neural network retrieval approach. We refer to Van Damme et al. (2017, 2021) TS2 for a detailed description of the algorithm. For CO, we used the product obtained with the FORLI v20140922 retrieval algorithm (Hurtmans et al., 2012). Given the absence of hourly or even daily observations of NH_3 concentrations in sub-Saharan Africa, the detection limit of IASI is difficult to determine with certainty. However, the region experiences high thermal contrast, and IASI seems to be able to reliably observe NH_3 down to 1 to 2 ppb at the surface (Clarisse et al., 2009; Van

Damme et al., 2014b). We gridded the Level-2 IASI NH$_3$ and CO products to $0.5° \times 0.5°$ resolution. We used a conventional binning approach based on the center of each satellite footprint. We did not apply an averaging weight. Quality control procedures were followed as detailed in van Damme et al. (2017, 2021). Specifically, the screening of retrievals included filtering of retrievals where cloud cover is over 10 %, where the total column density is below zero and the absolute value of the hyperspectral range index (HRI) is above 1.5, and where the ratio of the total column density to HRI is larger than 1.5×10^{16} molecules cm^{-2}.

The IASI products have been validated using ground-based Fourier transform infrared (FTIR) observations of NH$_3$ total columns, with robust correlations at sites with high NH$_3$ concentrations but lower at sites where atmospheric concentrations approach IASI's detection limits (Dammers et al., 2016; Guo et al., 2021). Compared to the FTIR observations, total columns from previous IASI NH$_3$ products (IASI-LUT and IASI-NNv1) are biased low by ~ 30 % which varies per region depending on the local concentrations. Although FTIR observations are absent from Africa, earlier work has shown fair agreement between previous versions of IASI total column densities and surface observations of NH$_3$ using passive samplers across the International Network to study Deposition and Atmospheric chemistry in AFrica (INDAAF) network in West Africa (Van Damme et al., 2015), including in observations of seasonal variation (Hickman et al., 2018; Ossohou et al., 2019). Validation of the IASI CO product using surface, aircraft, and satellite observations have found total columns to have an error that is generally below 10 %–15 % in the tropics and midlatitudes (George et al., 2009; Kerzenmacher et al., 2012; Pommier et al., 2010; De Wachter et al., 2012). The IASI NH$_3$ and CO products were used for the years 2008 – the first full year of data available – to the end of 2018. Random errors in observations can be assumed to cancel out in the annual mean, which is what we used in our analysis. With the assumption that random errors cancel out, only systematic errors related to tropospheric vertical column contents remain; these systematic errors do not contribute to uncertainty in trend analyses. In addition, we first take monthly averages based on all daily observations within a given month before calculating annual means to minimize any potential effects of temporal variability in cloud cover.

- The Tropical Rainfall Measuring Mission (TRMM) daily precipitation product (3B42) is based on a combination of TRMM observations, geosynchronous infrared observations, and rain gauge observations (Huffman et al., 2007). Independent rain gauge observations from West Africa have been used to validate the product, with no indication of bias in the product (Nicholson et al., 2003).

- The NOAA Global Surface Temperature Dataset, a 0.5° gridded monthly 2 m land surface temperature product (Fan and van den Dool, 2008), is based on a combination of station observations from the Global Historical Climatology Network version 2 and the Climate Anomaly Monitoring System (GHCN_CAMS) and uses an anomaly interpolation approach which relies on observation-based reanalysis data to derive spatiotemporal variation in temperature lapse rates for topographic temperature adjustment.

- The 500 m MCD64A1 collection 6 Moderate Resolution Imaging Spectroradiometer (MODIS) burned-area product for the period 2008–2018 (Giglio et al., 2018), with the burned-area data aggregated by month and gridded to 0.25° resolution; the data do not include burned area from small fires.

- The MODIS MCD12C1 (collection 5) land cover product provides the percentage of cropped area in each 0.25° grid cell (Friedl et al., 2002). In Africa, agriculture is often practiced in complex mosaics of agricultural and natural land cover, so we used both the crop and crop–natural area mosaic MODIS classifications as agricultural area in our analysis.

- We also used data on the spatiotemporal distribution of armed conflict events from the Armed Conflict Location & Event Data Project (ACLED; Raleigh et al., 2010). We included data for both violent and non-violent conflict events over the period 2008–2018.

2.2 Sudd wetland extent

Monthly flooded area extents of the Sudd Wetland, South Sudan from 2000 to 2017 were derived from 8 d composite MODIS land surface reflectance imagery (MOD09A1); data from 2005 through 2017 were used in the analyses. We refer to Di Vittorio and Georgakakos (2018) for a detailed description of the classification procedure designed to retrieve these data. In summary, monthly flood maps were obtained through a two-stage classification procedure. The first stage used the full 18-year dataset to produce a wetland land cover map that distinguishes between wetland vegetation classes and their flooding regimes (permanently flooded, seasonally flooded, or non-flooded). The second stage compares seasonally flooded pixels from each vegetation class to their non-flooded counterparts on a monthly basis to identify the timing and duration of flooding for each pixel. These data were originally derived to calibrate a hydrologic model of the Sudd that is dependent on Nile flows (Di Vittorio and Georgakakos, 2021); therefore, a connectivity algorithm was applied to ensure that all flooded pixels were physically connected to the Nile River. A few adjustments have been

made to the previously published dataset for the application of this study. The classification algorithm has been improved to more accurately capture the interannual fluctuations in the permanently flooded areas. The dataset was also extended through 2017, and the total flooded area was quantified prior to applying the connectivity algorithm. The magnitudes of the monthly flooded area estimates are now substantially larger because they include areas flooded from local runoff in addition to areas flooded by the Nile River.

2.3 Spatial and national analyses

We evaluated spatial relationships between mean annual tropospheric NH_3 concentration and several independent variables at 0.25° TS3 resolution: population density, livestock density, and cropped area. Population density and livestock density data are not available as time series suitable for trend analysis, so we use single-year values in our analyses. We calculated population density based on the 2017 version of the US Department of Energy's Gridded Landscan population dataset (Dobson et al., 2000; available at https://landscan.ornl.gov, last access: 2 November 2020). Livestock density was based on the FAO global gridded livestock dataset for the year 2007 (Robinson et al., 2014). Before analysis, we converted the livestock densities of chickens, goats, pigs, and sheep to tropical livestock units (TLUs), using values of 0.01, 0.1, 0.2, and 0.1 TLU, respectively; North African cattle were converted using a factor of 0.7, whereas sub-Saharan cattle were converted using a factor of 0.5 (Chilonda and Otte, 2006). For cropped area, we used the MODIS MCD12C1 (collection 5) land cover product as described above. We conducted spatial analyses by establishing a map of 3° grid cells and calculating the correlation between the value of each independent variable and NH_3 for all 0.5° grid cells within the larger grid cells ($N = 36$ TS4 including water grid cells, though these were excluded from the analysis).

National data on annual livestock numbers, crop production, and fertilizer N use were obtained from the UN Food and Agriculture Organization FAOSTAT for 51 African countries (FAO, 1997 TS5). Livestock data consisting of sheep, goats, cattle, and pigs were converted to tropical livestock units as described above, and buffaloes were converted using a conversion factors of 0.7 (Chilonda and Otte, 2006). National emissions of CO_2 were obtained from World Bank Open Data (World Bank, 2019). National-level mean annual cropland area, burned area, and atmospheric NH_3 and CO concentrations were also calculated for each of the 51 countries from the spatial datasets described above. Countries were sorted into three bins based on whether their relative change in mean annual NH_3 concentration was low, medium, or high, and means and standard errors were calculated for each of the three 17-country bins.

Linear trend analyses were conducted using linregress from the scipy.stats package in Python v3.6.3. Statistical analyses of national-scale data were conducted using ANOVA in R. Data were log- or rank-transformed when necessary to meet the assumptions of ANOVA. Values of α for treatment comparisons following significant ANOVA results were corrected for multiple testing using Benjamini–Hochberg corrections.

3 Results and discussion

3.1 Continental distributions and trends

Mean annual NH_3 concentrations for 2008–2018 are highest across the savannas and forest–savanna mosaics in north equatorial Africa and especially in West Africa; there are smaller regional hotspots in the Lake Victoria basin region, South Sudanese wetlands, and along the Nile delta and river (Fig. 1a). Parts of these regions experience substantial biomass burning (Fig. 1e), high livestock densities (Fig. 1g), and/or high cropland cover (Fig. 1h), all of which can contribute to NH_3 emissions. The high concentrations in West Africa, which is one of the major global NH_3 hotspots (Van Damme et al., 2018), are likely the result of biomass burning emissions. Biomass burning emissions tend to drive seasonal variation in NH_3 vertical column densities (VCDs) in West Africa, with the largest emissions occurring late in the dry season and early rainy season (Hickman et al., 2021b). In addition to local emissions, biomass burning emissions and their reactive products are transported to the coast of West Africa during both the Northern Hemisphere rainy season, when they are transported from central and Southern Africa, and during the dry season, when they are transported from biomass burning regions to the east (Sauvage et al., 2007).

In addition to being hotspots of mean NH_3 concentrations, some of these regions have also experienced increases in NH_3 concentrations from 2008 to 2018 (Fig. 1b). Like Warner et al. (2017) and Van Damme et al. (2021), we observed some increases in the northern grasslands, central African forests, and the Nile region, but we also observe trends in the Lake Victoria basin region, which Warner et al. (2017) did not, but Van Damme et al. (2021) did. Also in contrast to Warner et al. (2017) but in line with Van Damme et al. (2021), we observe a prominent decline in NH_3 VCDs over South Sudan (Figs. 1b, S1). Most areas with trends are significant at $P = 0.2$ or higher (Fig. S1).

The Nile region exhibits elevated NH_3 concentrations and a modest positive trend over the observation period (Fig. 1a, b). This trend appears largely to be related to agriculture and livestock: in a spatial analysis, snapshots of livestock densities and of population densities are both positively related to changes in NH_3 VCDs (Fig. 2). Although there is not a positive relationship between agricultural area and NH_3 VCDs over the Nile region from 2008 to 2018, Egypt's population increased by roughly 25 % over that period (World Bank, 2019), and fertilizer N use increased by

Atmos. Chem. Phys., 21, 1–15, 2021 **https://doi.org/10.5194/acp-21-1-2021**
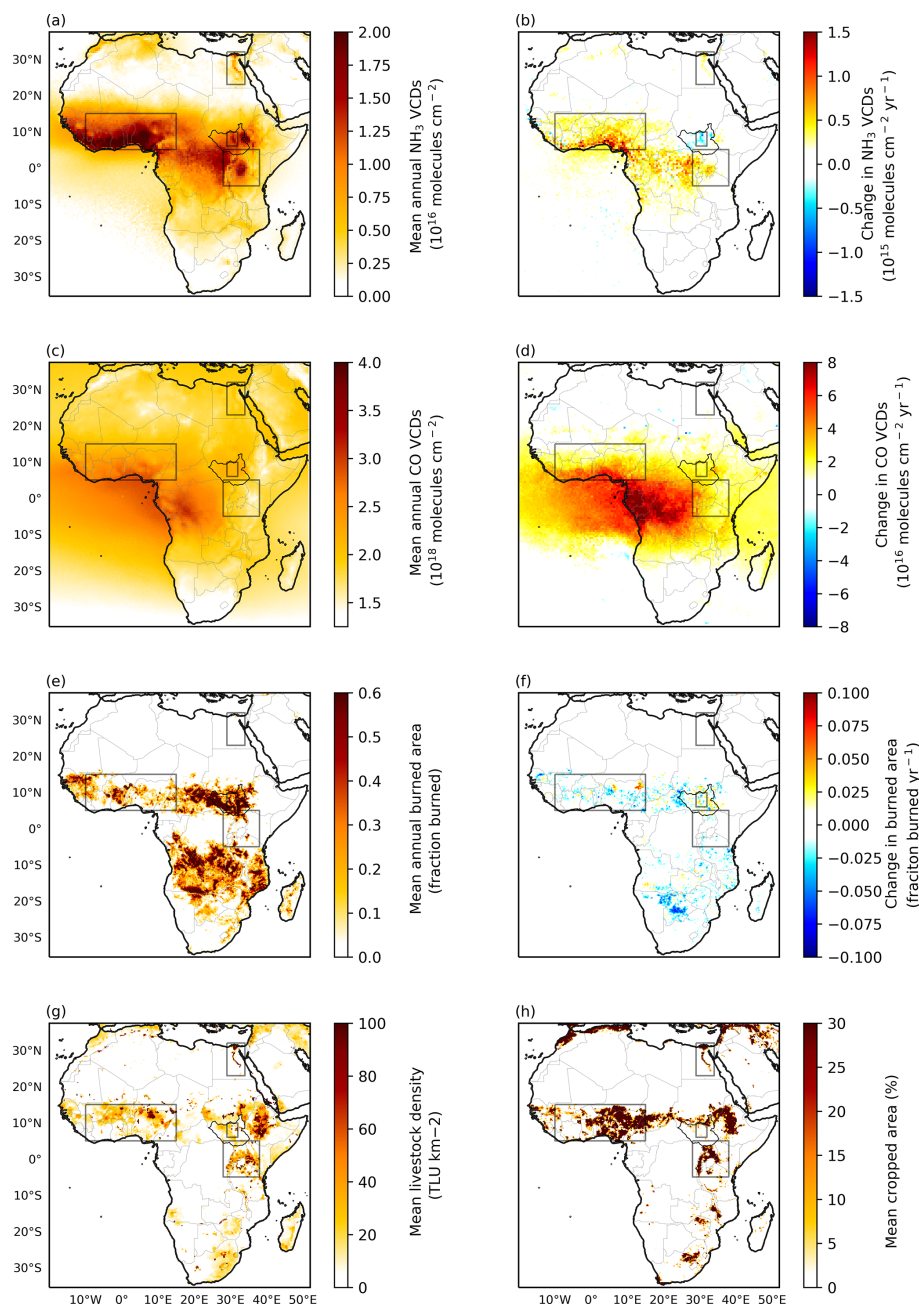
Figure 1. Annual averages and trends in atmospheric NH$_3$ VCDs, CO VCDs, and burned area as well as spatial distribution of livestock density and cropped area across seven sub-Saharan African ecoregions. Mean annual **(a)** and trend **(b)** in atmospheric NH$_3$ VCDs from IASI for the period 2008 through 2018. Mean annual **(c)** and trend **(d)** in annual atmospheric CO VCDs from IASI for the same period. Mean annual **(e)** and trend **(f)** in annual burned area from MODIS for 2008–2018. Livestock densities for 2007 from the FAO **(g)**, and mean cropped area from MODIS for 2008–2018 **(h)**. The border of South Sudan is highlighted in black, and several regions are boxed: the Nile region at 30° N, the Sudd wetland in South Sudan, the Lake Victoria region at the Equator, and West Africa centered around 10° N.

roughly 8 % after a decline in use between 2004 and 2007 (FAO, 1997TS6), suggesting that increased agricultural N inputs may be contributing to the trend. We evaluate the other regions in more detail below.

3.2 West Africa

The increasing trend in NH$_3$ VCDs over West Africa is centered over Nigeria and the southern coast and to a lesser extent across parts of the wet savanna (Fig. 1b). Increases in NH$_3$ VCDs tend to be higher in grid cells with higher pop-
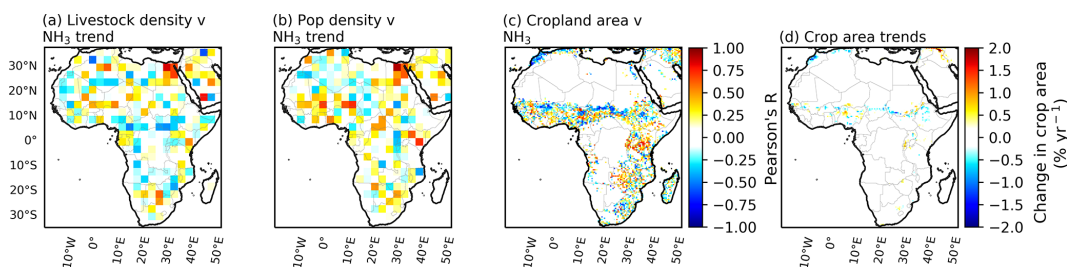
Figure 2. Relationships between NH_3 trends and livestock density, population density, and cropland area as well as changes in cropland area. Spatial correlations between changes in annual atmospheric NH_3 VCDs and livestock density **(a)** and population density **(b)**. Correlation between cropland area and NH_3 VCDs for 2008 through 2018 **(c)**. Change in crop area for 2008 through 2018 **(d)**. The NH_3 and crop area trends are based on data for 2008 through 2018, livestock density data are for the year 2007, and population density data are for the year 2017.

ulation densities in Nigeria and other parts of West Africa (Fig. 2b), suggesting a possible anthropogenic influence. The spatial distribution of the mean annual NH_3 trend is overlapped by a substantial increase in mean annual CO VCDs (Fig. 1b, d), pointing to a biomass burning source, as is also the case in central Africa. Earlier studies have found substantial declines in annual burned area across the north equatorial African biomass burning region as detected by MODIS (Andela et al., 2017; Andela and van der Werf, 2014) and related declines in NO_2 VCDs across the region (Hickman et al., 2021a), which would seem to stand in contrast to the increasing CO and NH_3 trends observed here.

However, the annual decline in burned area and NO_2 VCDs is characterized by heterogeneity when considering individual months. In West Africa, the dry season is typically November to February or March. During the transition from the dry to rainy season in February and March, NO_2 VCDs exhibit increasing rather than decreasing trends in West Africa, though burned-area patterns are not as clear when 2018 is included (Hickman et al., 2021a; Figs. S2, S3). Although these increases in NO_2 VCDs are small in the annual context, they occur at a time of year when biomass burning combustion is less complete, potentially due to greater fuel moisture and declining fire radiative power (Hickman et al., 2021a; Zheng et al., 2018). These conditions would lead to greater emissions of less oxidized species such as CO and NH_3, rather than the more fully oxidized species such as CO_2 and NO_2 that dominate emissions during the peak of the biomass burning season (Figs. S2, S4). Indeed, our observations suggest that much of the increasing NH_3 trend occurs during this transitional period, with NH_3 VCDs increasing by roughly $6\%\,yr^{-1}$ for all of Nigeria during February and March (Figs. 3, S5; $p<0.01$). Variation in NH_3 VCDs are positively correlated with CO VCDs (Figs. 4a, S6), which are also increasing during this period (Figs. 4c, S4).

These correlations imply a biomass burning source for the increasing NH_3 VCDs in West Africa; although the burned-area trends are not as clear, it is important to note that MODIS undercounts burned area during this time of year by

a factor of 3 to 6 and so would be less sensitive to trends (Ramo et al., 2021; Roteta et al., 2019). Although there is considerable gas flaring in Nigeria, gas flaring emissions have exhibited long-term negative trends (Doumbia et al., 2019). In addition, although NO_2 VCDs were found to decrease across the productive savannas of West Africa, regions of increasing NO_2 VCDs were observed over large parts of Nigeria, further suggesting that there may be increases – or at least smaller decreases – in biomass burning in the country (Hickman et al., 2021a). It is unlikely that changes in chemical sinks – specifically, the formation of nitrate aerosols in reactions with NO_x or sulfate – are responsible for the increasing trend: the observed increase in NO_2 VCDs observed during February and March would be expected to lead to a shorter NH_3 lifetime and decreasing VCDs. In addition, emissions of SO_2 are relatively low in West Africa, with moderate emissions occurring in Nigeria, but neither emissions nor lifetime exhibits clear seasonal variation (Lee et al., 2011).

Small agricultural fires are likely an important contributor to the increasing NH_3 VCDs during the dry-to-rainy-season transitional period – a period when agricultural fires are common in the region (Korontzi et al., 2006). There are large numbers of small fires that are not detected by MODIS during these months: as noted above, estimates of burned area during February, March, and April are revised upwards by roughly a factor of 3 to 6 over MODIS when small fires are included (Ramo et al., 2021; Roteta et al., 2019). Many of these small fires are likely related to agricultural field preparation prior to planting (Gbadegesin and Olusesi, 1994), which typically takes place in March or April (Vrieling et al., 2011; Yegbemey et al., 2014). An increase in fires during this transitional period is also consistent with one of the primary mechanisms behind the overall decline in burned area: roughly half of the decline is attributed to increased population density and the expansion of agricultural area, which contributes to the anthropogenic suppression of larger fires (Andela et al., 2017; Andela and van der Werf, 2014). This agricultural expansion, however, can be
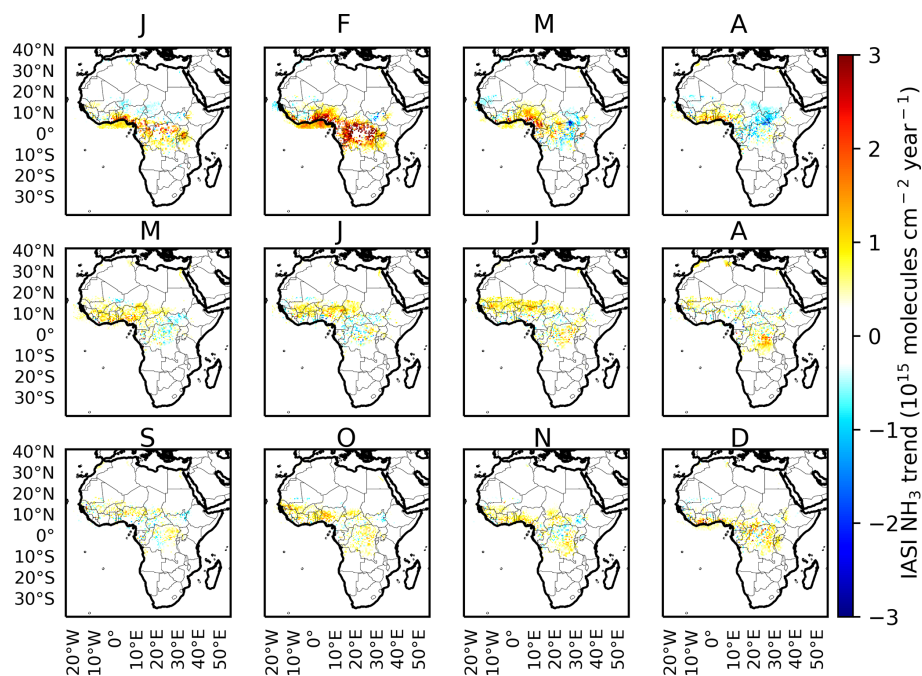
Figure 3. Change in mean monthly atmospheric NH$_3$ VCDs for the period 2008 through 2018. Grid cells where mean annual NH$_3$ VCDs for the entire period are under 5×10^{15} molecules cm^{-2} are not displayed. Results significant at $P = 0.05$ are presented in Fig. S5.
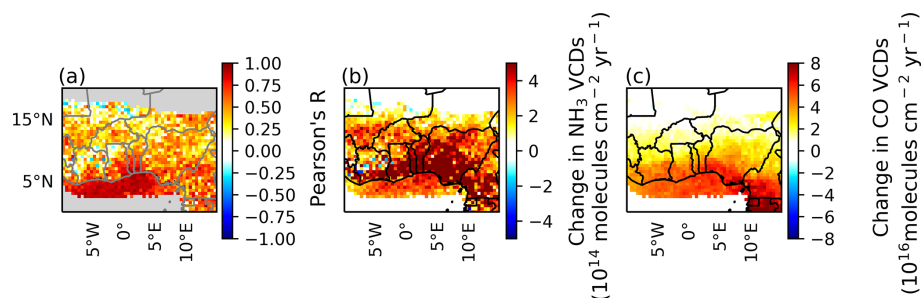
Figure 4. Correlation coefficient for the relationship between mean annual CO and NH$_3$ VCDs **(a)**, changes in NH$_3$ VCDs **(b)** and changes in CO VCDs **(c)** over 2008 through 2018 in West Africa. Grid cells where mean annual NH$_3$ VCDs for the entire period are under 5×10^{15} molecules cm^{-2} are not displayed. Results significant at $P = 0.05$ for the entire continent are presented in Fig. S6.

expected to be accompanied by increases in small fires used for the removal of stubble or harvest byproduct (Gbadegesin and Olusesi, 1994), leading to the increased emissions during the rainy-to-dry-season transition observed here.

Globally, agricultural emissions from fertilized soils and livestock excreta are the largest source of NH$_3$ (Bauer et al., 2016), and Warner et al. (2017) suggest that national-scale changes in fertilizer use could explain the NH$_3$ trend over Nigeria. However, as noted above, much of the increase in West Africa occurs prior to the start of the planting season – before fertilizer is applied – and appears likely to be due to biomass burning emissions instead, potentially related to field preparation. Fertilizer or manure may make a contribution to the increasing trend later in the year, as NH$_3$ VCDs increase in the wet savanna during May, June, and

July (Fig. 3), though there are also significant correlations between NH$_3$ and CO VCDs (Fig. 4), suggesting that biomass burning may continue to play an important role. However, average N fertilizer use in West Africa is universally under 40 kg N ha^{-1} yr^{-1}, typically under 20 kg N ha^{-1} yr^{-1}, and is under 10 kg N ha^{-1} yr^{-1} in Nigeria – over an order of magnitude lower than rates in Europe, the United States, and China (FAO, 1997 TS7). Although percentage changes in fertilizer use are substantial, in absolute terms they represent increases of less than 2 kg N ha^{-1} yr^{-1} and frequently less than 1 kg N ha^{-1} yr^{-1}, a relatively small but perhaps not entirely trivial perturbation to the N cycle: between 2000 and 2007, total N deposition averaged 8.38 kg N ha^{-1} yr^{-1} in wet savanna and 14.75 kg N ha^{-1} yr^{-1} in forest ecosystems based on surface sampling sites (Galy-Lacaux and Delon,

2014), and biological N fixation in tropical and wet savannas has been estimated as ranging from 16 to 44 kg N ha^{-1} yr^{-1} (Bustamante et al., 2006). These estimates suggest that fertilizer increases may represent a 1 % to 2 % annual increase in N inputs. But given the small magnitude of fertilizer applications, it appears unlikely that changes in fertilizer use can explain the entirety of NH$_3$ increases during the growing season. Our analyses do suggest that livestock may contribute to increasing NH$_3$ VCDs over the Sahel, from roughly 15 to 18° N (Fig. 2a). However, many of these pixels are also those where population density appears to be playing a role (Fig. 2b) and where correlations between NH$_3$ and CO VCDs are present during the transition from the dry to rainy season (Fig. S7), which may reflect a contribution from agricultural fires.

3.3 South Sudan

The most notable declining trend in NH$_3$ VCDs occurs in South Sudan over the Sudd wetlands at a rate of over 2 % yr^{-1} TS8 (Fig. 1b; $p = 0.20$). It appears that this decline is related to interannual variation in the flooded extent of the Sudd, a vast wetland that connects the White and Blue Nile tributaries. Seasonal variation in inflow to the Sudd leads to variation in flooded extent: an area of roughly 15 000 km^2 is permanently flooded, and another roughly 15 000 km^2 is temporarily flooded each year, with considerable interannual variation in the total flooded area (Di Vittorio and Georgakakos, 2018). Among other factors, drying soils should increase production and emissions of NH$_3$ from soils, as Eq. (1) is shifted to the right (Clarisse et al., 2019). Earlier work evaluating an NH$_3$ hotspot over Lake Natron in Tanzania found that the drying of seasonally flooded soils leads to large emissions of NH$_3$: as the waters of Lake Natron recede during the dry season each year and the surrounding mud flats dry out, NH$_3$ VCDs increase rapidly, with hotspots appearing over the mudflats (Clarisse et al., 2019). These elevated VCDs are attributed to multiple possible factors, including the effects of drying on concentrations of NH$_3$ in solution (which increases the concentration gradient with the atmosphere), reduced biological uptake of NH$_3$, convective transport of dissolved NH$_3$ from depth to the soil surface, and increased mineralization of labile organic matter (Clarisse et al., 2019).

We find the same clear seasonal relationship between wetland flooded extent and NH$_3$ concentrations over the Sudd – VCDs increase as waters recede from the temporarily flooded area, leading to annual maxima from February through May (Fig. 5a; bounding box of 29 to 31.5° E and 6 to 9.9° N TS9). Like in the entire country, seasonal variation in NH$_3$ VCDs over the Sudd follows variation in surface temperature, but NH$_3$ concentrations over the Sudd are substantially elevated compared to surrounding regions during this time of year but not others, suggesting that a mechanism in addition to temperature is contributing to the elevated emissions in the Sudd

during February through May, a period that spans the end of the dry season and start of the rainy season (Fig. S8). This conclusion is supported by an analysis of interannual variation in VCDs during the February through May period: interannual variation in NH$_3$ VCDs is largely decoupled from variation in temperature, but NH$_3$ VCDs appear to vary inversely with the amount of area that dries out each year (Fig. 5b). Over the period for which flooded-extent data are currently available for the Sudd, the minimum flooded extent tends to increase – that is, less area dries out each year – resulting in an overall decline in NH$_3$ VCDs. Linear regression reveals that this change in flooded extent explains a large proportion of the annual variation in NH$_3$ in the Sudd bounding box ($r = -0.64$, $p = 0.046$), as well as for the country as a whole ($r = -0.60$, $p = 0.065$). These analyses strongly suggest that the declining trend in NH$_3$ over the Sudd is a direct result of an overall increase in the minimum flooded extent over the observation period.

It is possible that conflict in South Sudan could contribute to the decline in NH$_3$ VCDs. In 2013, a civil conflict emerged in South Sudan that was ultimately responsible for the displacement of millions of people (Global Internal Displacement Monitoring Centre, 2020; World Bank, 2019) and the disruption of livestock migration patterns (Idris, 2018). However, these disruptions appeared only after the onset of the long-term change in NH$_3$ and appear unlikely to make an important contribution to the observed interannual variation (Supplement text, Figs. S9, S10).

It is unlikely that changes in chemical sinks are responsible for the decline in NH$_3$ VCDs. VCDs of tropospheric NO$_2$ are also decreasing in the region (Fig. S11), which is suggestive of less formation of particulate-phase ammonium rather than more. Anthropogenic SO$_2$ emissions in Africa in general and South Sudan in particular are very low (European Commission Joint Research Centre (JRC)/Netherlands Environmental Assessment Agency (PBL), 2016) and would not be expected to be emitted from the Sudd; more generally, the clear spatial association between the NH$_3$ trend and the Sudd (Figs. 1, S12) is strongly suggestive of changes in emissions rather than atmospheric processes being responsible for the trend.

3.4 Lake Victoria basin region

The Lake Victoria basin and its surroundings – an area including elevated mean NH$_3$ VCDs – exhibit an increasing NH$_3$ trend (Figs. 1b, 6, S13), which appears to be the result of increasing agricultural activity in the area. The region includes a high and increasing density of agricultural land (Figs. 1h, 2d, S14), and these increases in cropped area are positively correlated with increases in NH$_3$ VCDs across much of the region (Fig. 2c). The northern and southern halves of the Lake Victoria region – which straddles the Equator – have distinct growing seasons: in the north, the season generally starts in April, whereas in the south, it starts

Atmos. Chem. Phys., 21, 1–15, 2021   https://doi.org/10.5194/acp-21-1-2021
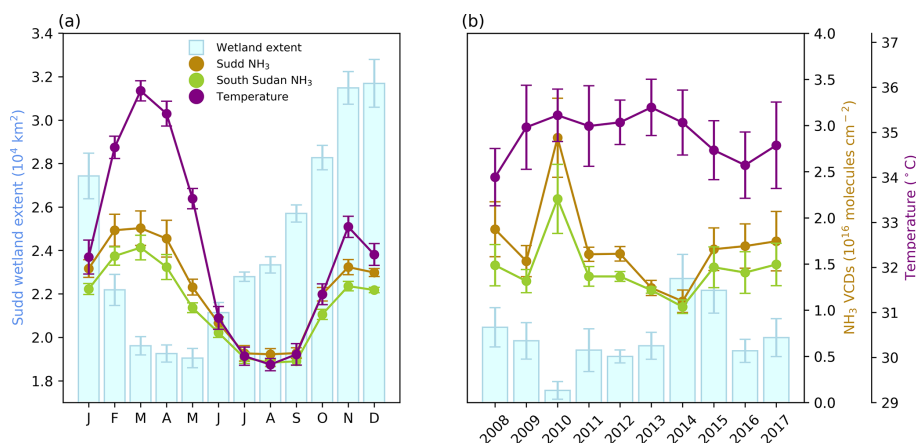
Figure 5. Mean **(a)** monthly and **(b)** February through May annual mean flooded extent of the Sudd, surface temperatures over South Sudan, and NH$_3$ VCDs over the Sudd and the entirety of South Sudan for the period 2008 through 2017.

in November or December (Vrieling et al., 2011). Some of the long-term trend reflects this seasonality, with increases in the north and south occurring during their respective growing seasons (Figs. 3, S15). Fertilizer use in the Lake Victoria region is low: national averages range from about 1 to 3 kg nutrients ha^{-1} yr^{-1} in Uganda to about 35 to 40 kg nutrients ha^{-1} yr^{-1} in Kenya (Elrys et al., 2019; World Bank, 2019); to put these numbers in context, Organization for Economic Cooperation and Development (OECD) countries use about 135–140 kg nutrients ha^{-1} yr^{-1} (World Bank, 2019). Although rates of fertilizer use have increased by substantial proportions, the absolute amount of increase is relatively small, typically roughly 1 to 10 kg nutrients decade^{-1}. Unlike in West Africa, however, interannual variation in burned area (Figs. 6, S16) does not exhibit a clear relationship with changes in NH$_3$ VCDs. Consequently, we expect that both the expansion and intensification of agriculture in the region contribute to the increasing NH$_3$ VCDs.

We note that there is a negative correlation between cropland area and NH$_3$ VCDs in Uganda, north of Lake Victoria (Fig. 6b). We expect this is a consequence of the extremely low fertilizer use in Uganda (Masso et al., 2017), which leads to depletion of soil N – and thus substrate for ammonia volatilization – over time (Cobo et al., 2010).

We also note that there is an apparent increase in NH$_3$ VCDs over the lake itself. It is important to note that differences in conditions over the lake and adjacent land cover – e.g., emissivity, thermal contrast, etc. – contribute to substantial differences in mean retrieved NH$_3$ VCDs over the lake relative to the surrounding land surface. Both monthly and interannual variation in NH$_3$ VCDs over Lake Victoria correspond closely to variation in NH$_3$ VCDs over the surrounding land surface (Figs. S17, S18), suggesting that the trend over the lake results from transport of NH$_3$ emitted from surrounding land surface.

3.5 National-scale relationships

Examining relationships at a national scale can provide insight into relationships between changes in agricultural or biomass burning and changes in atmospheric NH$_3$ VCDs at larger scales. When grouping countries into three bins based on their annual percentage changes in NH$_3$ VCDs, there is some evidence for a broad relationship between livestock and NH$_3$ VCDs at the national scale (Fig. 7). The rate of change in national-scale NH$_3$ VCDs varies significantly among bins ($p<0.001$; rank transformed, though note that residuals may still deviate from normality). The annual percentage changes in livestock in TLUs vary significantly by bin ($p = 0.042$; rank transformed), with the middle bin higher than the bottom bin ($p = 0.1$) and the high bin higher than the bottom bin ($p = 0.06$). Annual percentage changes in fertilizer N ($p = 0.58$) and crop production ($p = 0.62$; rank transformed) did not vary by bin.

Instead of a direct agricultural relationship with changes in NH$_3$ VCDs, there is the possibility that changes in biomass burning are associated with changes in NH$_3$ VCDs. Although the differences in the annual percentage change in burned area were not significant among bins ($p = 0.54$; rank transformed), the overall pattern is consistent with earlier results finding that a reduction in burned area across the northern biomass burning region was associated in part with the expansion of agriculture and presumed anthropogenic suppression of fire (Andela et al., 2017; Andela and van der Werf, 2014). However, burned area as measured by MODIS is likely an imperfect predictor for NH$_3$ emissions – as noted previously, MODIS underestimates burned area by a factor of 3 to 6 during shoulder seasons (Roteta et al., 2019), which is when fires are expected to emit more reduced species such as NH$_3$ (Zheng et al., 2018). In contrast to burned area, the annual change in column densities of CO – which tends to be co-emitted with NH$_3$ from fires – differed significantly
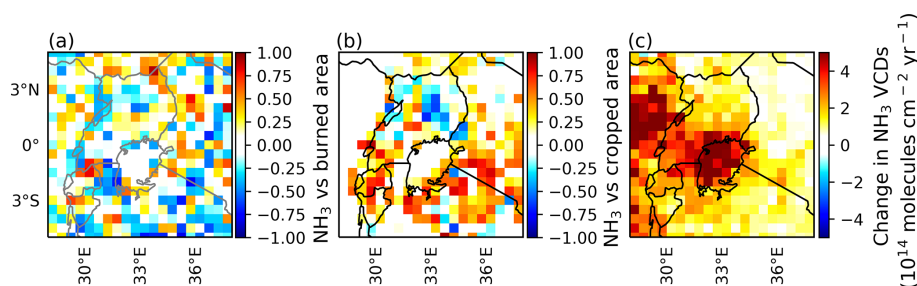
Figure 6. Changes in NH$_3$ VCDs and their relationship with burned area and cropped area over the Lake Victoria region for the 2008 through 2018 period. **(a)** Correlation coefficients for the relationship between NH$_3$ VCDs and burned area. **(b)** Correlation coefficients for the relationship between NH$_3$ VCDs and cropped area, including mosaics of crops and natural vegetation cover. **(c)** Changes in NH$_3$ VCDs.
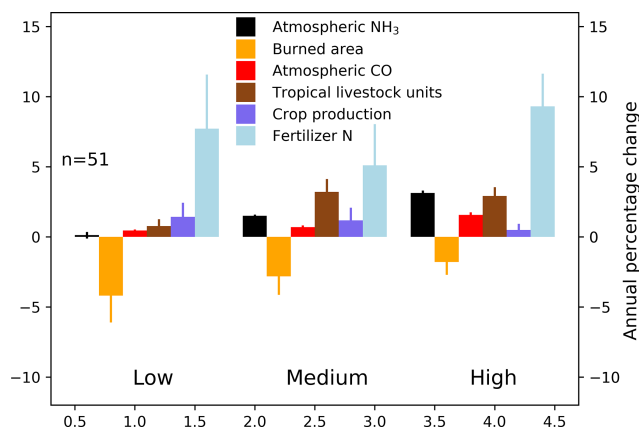
Figure 7. Annual percentage changes in national mean annual NH$_3$ VCDs, burned area, CO VCDs, livestock, crop yield, and fertilizer N use for African countries with low, medium, or high rates of NH$_3$ VCD change. Error bars represent the standard error of the mean. See Table S1 for the list of countries in each bin and Fig. S19 for an expanded set of variables.

among bins ($p<0.001$; rank transformed) and was significantly higher in the high bin than in the low or medium bins ($p<0.001$, post hoc tests). The higher annual CO changes in the high bin could be related to larger anthropogenic fossil fuel emissions, but we see no difference among bins in growth rates of CO$_2$ emissions ($p = 0.48$; Fig. S19); such a difference would be expected if differences in economic development were responsible for the CO differences. These results leave open the possibility that changes in either biofuel emissions or biomass burning emissions – perhaps from smaller fires not observed in the MODIS burned-area product – may be primarily responsible for the difference in CO between bins and may be contributing to the differences in NH$_3$ between bins. Changes in NO$_2$ VCDs and SO$_2$ concentrations can affect the lifetime of NH$_3$ (the latter by changing SO$_4$ concentrations) but do not appear to make an important contribution to the observed trends in NH$_3$ VCDs among bins (Fig. S19, Supplement text). Temperature, likewise, does not appear to play an important role (Supplement text).

4   Conclusion

Using IASI, we have observed both increases and decreases in atmospheric NH$_3$ VCDs in different regions in Africa between 2008 and 2018, with different factors affecting trends in different regions.

We observed increases in NH$_3$ VCDs in West Africa, which earlier work had concluded was likely related to increased fertilizer use. Fertilizer is not typically applied in West Africa until the start of the growing season – often April – but we find that much of the NH$_3$ increase occurs during February and March, suggesting that increasing fertilizer use is unlikely to provide a complete explanation for the NH$_3$ trend. Agriculture may nevertheless play a role, with enhanced burned area and especially CO concentrations in February suggestive of increased burning of crop stubble in preparation for planting during this time of year. Fires in this region tend to emit a greater proportion of less oxidized species such as NH$_3$ at the end of the dry season, consistent with a biomass burning source for the increasing NH$_3$ VCDs.

Decreases in NH$_3$ VCDs were largest in South Sudan, especially over the Sudd wetland, where NH$_3$ VCDs vary seasonally with the extent of area flooded. As the temporarily flooded areas of the Sudd dry out each year, NH$_3$ VCDs increase as reduction in soil moisture drives increased production and volatilization of NH$_3$. The area of the Sudd that is flooded each year varies, and from 2008 until 2015, the area that remains flooded during the dry season generally increased, producing a positive overall trend for the period of 2008 through 2017. This increase in the dry-season flooded area drove a decrease in NH$_3$ VCDs: with less soil drying out, the seasonal maxima in NH$_3$ VCDs were lower. Although it is possible that conflict in South Sudan could contribute to changes in NH$_3$ VCDs, the timing and distribution of conflict events and human displacement suggest that other factors are likely more important.

Modest increases in NH$_3$ VCDs were observed in the Lake Victoria region. This region has experienced increases in agricultural area during the IASI observation period, and these changes explained a large proportion of the variation in

NH$_3$ VCDs across large patches of the region, where biomass burning could not. We expect that both expansion and intensification of agriculture in this region could contribute to the positive NH$_3$ trend.

Considering national-scale statistics, comparisons between equally sized bins of 17 countries each suggested that changes in biomass burning emissions and livestock emissions could contribute to differences in NH$_3$ VCDs among countries, but variables related to cropped agriculture such as cropped area or fertilizer N use did not appear to be important factors at this scale. This may be because although fertilizer use has been increasing in sub-Saharan Africa, it remains extremely low relative to other continents and relative to the levels needed to attain food security. Average fertilizer use in most countries in the region is under 20 kg N ha^{-1} yr^{-1} and sometimes less than 5 kg N ha^{-1} yr^{-1}. Although recommended fertilizer rates are lower in most African countries than in the US or Europe, increasing N inputs to 50 or 100 kg N ha^{-1} yr^{-1} would represent a major perturbation to the regional N cycle and potentially a large new source of NH$_3$ to the atmosphere. West Africa is already a global NH$_3$ hotspot (Van Damme et al., 2018), suggesting that encouraging policies that can help to limit NH$_3$ emissions during the early stages of agricultural intensification in Africa may help mitigate potential impacts on the atmosphere. Fortunately, agricultural practices such as subsurface application of fertilizer, which is already being promoted to smallholder farmers, can serve to both limit NH$_3$ emissions and also help to increase crop yields.

These past and anticipated future trends also make the case for expanding capacity for atmospheric monitoring in sub-Saharan Africa. Although long-term monitoring networks have been established across West Africa (Adon et al., 2010; Ossohou et al., 2019) and in South Africa (Conradie et al., 2016) as part of the INDAAF network, it is mainly focused on deposition and the spatiotemporal resolution of surface measurements is very coarse when compared to the data available in other parts of the world, which will limit our ability to understand how agricultural and socioeconomic development in Africa affect the atmosphere. Satellite observations can help to bridge some of these data gaps but have their own spatiotemporal limitations and would further benefit from additional high-quality surface observations for the evaluation of retrieval products.

Data availability. All data used in this study are available from public sources, with the exception of Sudd wetland extent, which is available by request from Courtney Di Vittorio. The IASI NH$_3$ and CO data are available from IASI at https://iasi.aeris-data.fr/NH3R-ERA5_IASI_A_data/ (Clarisse et al., 2021 TS10) and https://iasi.aeris-data.fr/CO_IASI_A_data/ (Hurtmans et al., 2021 TS11). The NOAA Global Surface Temperature Dataset is available at https://doi.org/10.25921/9qth-2p70 (Zhang et al., 2021 TS12). MODIS burned-area data are avail-

able from https://doi.org/10.5067/MODIS/MCD64A1.006 (Giglio et al., 2015). MODIS agricultural area is available at https://doi.org/10.5067/MODIS/MCD12C1.006 (Friedl and Sulla-Menashe, 2015). TRMM 3B42 precipitation data are available from https://doi.org/10.5067/TRMM/TMPA/MONTH/7 (Tropical Rainfall Measuring Mission (TRMM), 2011). The Gridded Livestock of the World data are available from https://doi.org/10.7910/DVN/BLWPZN (Gilbert et al. 2018a), https://doi.org/10.7910/DVN/33N0JG (Gilbert et al. 2018b), https://doi.org/10.7910/DVN/OCPH42 (Gilbert et al. 2018c), https://doi.org/10.7910/DVN/GIVQ75 (Gilbert et al. 2018d), https://doi.org/10.7910/DVN/SUFASB (Gilbert et al. 2018e), https://doi.org/10.7910/DVN/5U8MWI (Gilbert et al. 2018f). Population density data for 2017 are available at https://landscan.ornl.gov/downloads/2017 (Rose et al., 2018). FAO national crop production and fertilizer N data are available at http://www.fao.org/faostat/en/#data/QCL, http://www.fao.org/faostat/en/#data/RFN (Food and Agriculture Organization of the United Nations, 2021a, b TS13). Data on conflict events from ACLED are available at https://acleddata.com/data-export-tool/ (Armed Conflict Location & Event Data Project, 2019). World Bank National statistics on refugees and internally displaced people are available at https://data.worldbank.org/indicator/SM.POP.REFG.OR (The World Bank, 2019), https://data.worldbank.org/indicator/VC.IDP.TOCV (Global Internal Displacement Monitoring Centre, 2020), and https://data.worldbank.org/indicator/VC.IDP.NWCV (United Nations High Commissioner on Refugees, 2020). TS14

Supplement. The supplement related to this article is available online at: https://doi.org/10.5194/acp-21-1-2021-supplement.

Author contributions. JEH designed the study, conducted the analysis, and wrote the paper. NA, ED, CADV, MO, CGL, KT, and SEB contributed to study design and edited the paper. LC, PFC, and MVD developed the original IASI trace gas retrievals and edited the paper.

Competing interests. The authors declare that they have no conflict of interest.

Acknowledgements. Jonathan E. Hickman's TS15 research was supported by an appointment to the NASA Postdoctoral Program at the NASA Goddard Institute for Space Studies administered by the Universities Space Research Association under contract with NASA.

Financial support. . TS16

Review statement. This paper was edited by Jayanarayanan Kuttippurath and reviewed by two anonymous referees.

References

Adon, M., Galy-Lacaux, C., Yoboué, V., Delon, C., Lacaux, J. P., Castera, P., Gardrat, E., Pienaar, J., Al Ourabi, H., Laouali, D., Diop, B., Sigha-Nkamdjou, L., Akpo, A., Tathy, J. P., Lavenu, F., and Mougin, E.: Long term measurements of sulfur dioxide, nitrogen dioxide, ammonia, nitric acid and ozone in Africa using passive samplers, Atmos. Chem. Phys., 10, 7467–7487, https://doi.org/10.5194/acp-10-7467-2010, 2010.

AGRA: AGRA in 2008: Building on the New Momentum in African Agriculture, Alliance for a Green Revolution in Africa, Nairobi, Kenya, 32 pp., 2009.

Andela, N. and van der Werf, G. R.: Recent trends in African fires driven by cropland expansion and El Niño to la Niña transition, Nat. Clim. Change, 4, 791–795, https://doi.org/10.1038/nclimate2313, 2014.

Andela, N., Morton, D. C., Giglio, L., Chen, Y., Van Der Werf, G. R., Kasibhatla, P. S., DeFries, R. S., Collatz, G. J., Hantson, S., Kloster, S., Bachelet, D., Forrest, M., Lasslop, G., Li, F., Mangeon, S., Melton, J. R., Yue, C., and Randerson, J. T.: A human-driven decline in global burned area, Science, 356, 1356–1362, https://doi.org/10.1126/science.aal4108, 2017.

Anker, H. T., Baaner, L., Backes, C., Keessen, A., and Möckel, S.: Comparison of ammonia regulation in Germany, the Netherlands and Denmark – legal framework, University of Copenhagen, Copenhagen, 23 pp., 2018.

Armed Conflict Location & Event Data Project (ACLED): Available Data TS17, ACLED [data set], available at: https://acleddata.com/data-export-tool/, last access: 14 November 2019.

Bauer, S. E., Tsigaridis, K., and Miller, R.: Significant atmospheric aerosol pollution caused by world food cultivation, Geophys. Res. Lett., 43, 5394–5400, https://doi.org/10.1002/2016GL068354, 2016.

Behera, S. N., Sharma, M., Aneja, V. P., and Balasubramanian, R.: Ammonia in the atmosphere: A review on emission sources, atmospheric chemistry and deposition on terrestrial bodies, Environ. Sci. Pollut. Res., 20, 8092–8131, https://doi.org/10.1007/s11356-013-2051-9, 2013.

Bouwman, A. F., Lee, D. S., Asman, W. A. H., Dentener, F. J., Van Der Hoek, K. W., and Olivier, J. G. J.: A global high-resolution emission inventory for ammonia, Global Biogeochem. Cy., 11, 561–587, 1997.

Bustamante, M. M. C., Medina, E., Asner, G. P., Nardoto, G. B., and Garcia-Montiel, D. C.: Nitrogen cycling in tropical and temperate savannas, Biogeochemistry, 79, 209–237, https://doi.org/10.1007/s10533-006-9006-x, 2006.

Cahoon, D. R., Stocks, B. J., Levine, J. S., Cofer, W. R., and O'Neill, K. P.: Seasonal distribution of African savanna fires, Nature, 359, 812–815, https://doi.org/10.1038/359812a0, 1992.

Chen, L.-W. A., Verburg, P., Shackelford, A., Zhu, D., Susfalk, R., Chow, J. C., and Watson, J. G.: Moisture effects on carbon and nitrogen emission from burning of wildland biomass, Atmos. Chem. Phys., 10, 6617–6625, https://doi.org/10.5194/acp-10-6617-2010, 2010.

Chilonda, P. and Otte, J.: Indicators to monitor trends in livestock production at national, regional and international levels, Livest. Res. Rural Dev., 18, 117, 2006.

Clarisse, L., Clerbaux, C., Dentener, F., Hurtmans, D., and Coheur, P. F.: Global ammonia distribution derived from infrared satellite observations, Nat. Geosci., 2, 479–483, https://doi.org/10.1038/ngeo551, 2009.

Clarisse, L., Van Damme, M., Gardner, W., Coheur, P.-F., Clerbaux, C., Whitburn, S., Hadji-Lazaro, J., and Hurtmans, D.: Atmospheric ammonia (NH_3) emanations from Lake Natron's saline mudflats, Sci. Rep., 9, 4441, https://doi.org/10.1038/s41598-019-39935-3, 2019.

Clarisse, L., Van Damme, M., and Coheur, P.-F.: Reanalyzed daily IASI/Metop-A ULB-LATMOS ammonia (NH3) L2 product (total column), [data set], available at: https://iasi.aeris-data.fr/NH3R-ERA5_IASI_A_data/, last access: February, 2021

Cobo, J. G., Dercon, G., and Cadisch, G.: Nutrient balances in African land use systems across different spatial scales: A review of approaches, challenges and progress, Agric. Ecosyst. Environ., 136, 1–15, https://doi.org/10.1016/j.agee.2009.11.006, 2010.

Conradie, E. H., Van Zyl, P. G., Pienaar, J. J., Beukes, J. P., Galy-Lacaux, C., Venter, A. D., and Mkhatshwa, G. V.: The chemical composition and fluxes of atmospheric wet deposition at four sites in South Africa, Atmos. Environ., 146, 113–131, https://doi.org/10.1016/j.atmosenv.2016.07.033, 2016.

Dammers, E., Palm, M., Van Damme, M., Vigouroux, C., Smale, D., Conway, S., Toon, G. C., Jones, N., Nussbaumer, E., Warneke, T., Petri, C., Clarisse, L., Clerbaux, C., Hermans, C., Lutsch, E., Strong, K., Hannigan, J. W., Nakajima, H., Morino, I., Herrera, B., Stremme, W., Grutter, M., Schaap, M., Wichink Kruit, R. J., Notholt, J., Coheur, P.-F., and Erisman, J. W.: An evaluation of IASI-NH_3 with ground-based Fourier transform infrared spectroscopy measurements, Atmos. Chem. Phys., 16, 10351–10368, https://doi.org/10.5194/acp-16-10351-2016, 2016.

Denier van der Gon, H. and Bleeker, A.: Indirect N_2O emission due to atmospheric N deposition for the Netherlands, Atmos. Environ., 39, 5827–5838, https://doi.org/10.1016/j.atmosenv.2005.06.019, 2005.

De Wachter, E., Barret, B., Le Flochmoën, E., Pavelin, E., Matricardi, M., Clerbaux, C., Hadji-Lazaro, J., George, M., Hurtmans, D., Coheur, P.-F., Nedelec, P., and Cammas, J. P.: Retrieval of MetOp-A/IASI CO profiles and validation with MOZAIC data, Atmos. Meas. Tech., 5, 2843–2857, https://doi.org/10.5194/amt-5-2843-2012, 2012.

Di Vittorio, C. A. and Georgakakos, A. P.: Land cover classification and wetland inundation mapping using MODIS, Remote Sens. Environ., 204, 1–17, https://doi.org/10.1016/j.rse.2017.11.001, 2018.

Di Vittorio, C. A. and Georgakakos, A. P.: Hydrologic Modeling of the Sudd Wetland using Satellite-based Data, J. Hydrol. Reg. Stud., 37, 100922, https://doi.org/10.1016/j.ejrh.2021.100922, 2021.

Dobson, J. E., Bright, E. A., Coleman, P. R., Durfee, R. C., and Worley, B. A.: A global population database for estimating populations at risk, Photogramm. Eng. Remote Sens., 66, 849–857, 2000.

Doumbia, E. H. T., Liousse, C., Keita, S., Granier, L., Granier, C., Elvidge, C. D., Elguindi, N., and Law, K.: Flaring

emissions in Africa: Distribution, evolution and comparison with current inventories, Atmos. Environ., 199, 423–434, https://doi.org/10.1016/j.atmosenv.2018.11.006, 2019.

Elrys, A. S., Abdel-Fattah, M. K., Raza, S., Chen, Z., and Zhou, J.: Spatial trends in the nitrogen budget of the African agro-food system over the past five decades, Environ. Res. Lett., 14, 124091, https://doi.org/10.1088/1748-9326/ab5d9e, 2019.

European Commission Joint Research Centre (JRC)/Netherlands Environmental Assessment Agency (PBL): Emission Database for Global Atmospheric Research (EDGAR), release version 4.3.1, [data set], available at: https://edgar.jrc.ec.europa.eu/gallery?release=v50_AP&substance=NH3§or=TOTALS, last access: 16 October 2016.

Fan, Y. and van den Dool, H.: A global monthly land surface air temperature analysis for 1948–present, J. Geophys. Res.-Atmos., 113, D01103, https://doi.org/10.1029/2007JD008470, 2008.

Food and Agriculture Organization of the United Nations: FAO-STAT Statistical Database, available at: http://www.fao.org/faostat/en/ (last access: 1 January 2020), 1997.

Food and Agriculture Organization of the United Nations: Crops and livestock products, FAOSTAT [data set], available at: http://www.fao.org/faostat/en/#data/QCL, last access: TS18 , 2021a. TS19

Food and Agriculture Organization of the United Nations: Fertilizers by Nutrient, FAOSTAT [data set], available at: http://www.fao.org/faostat/en/#data/RFN, last access: TS20 , 2021b. TS21

Friedl, M. and Sulla-Menashe, D.: MCD12C1 MODIS/Terra+Aqua Land Cover Type Yearly L3 Global 0.05Deg CMG V006, NASA EOSDIS Land Processes DAAC [data set], https://doi.org/10.5067/MODIS/MCD12C1.006, 2015.

Friedl, M. A., McIver, D. K., Hodges, J. C. F., Zhang, X. Y., Muchoney, D., Strahler, A. H., Woodcock, C. E., Gopal, S., Schneider, A., Cooper, A., Baccini, A., Gao, F., and Schaaf, C.: Global land cover mapping from MODIS: Algorithms and early results, Remote Sens. Environ., 83, 287–302, https://doi.org/10.1016/S0034-4257(02)00078-0, 2002.

Galy-Lacaux, C. and Delon, C.: Nitrogen emission and deposition budget in West and Central Africa, Environ. Res. Lett., 9, 125002 , https://doi.org/10.1088/1748-9326/9/12/125002, 2014.

Gbadegesin, A. and Olusesi, B. B.: Effects of land clearing methods on soil physical and hydrological properties in southwestern Nigeria, Environmentalist, 14, 297–303, 1994.

George, M., Clerbaux, C., Hurtmans, D., Turquety, S., Coheur, P.-F., Pommier, M., Hadji-Lazaro, J., Edwards, D. P., Worden, H., Luo, M., Rinsland, C., and McMillan, W.: Carbon monoxide distributions from the IASI/METOP mission: evaluation with other space-borne remote sensors, Atmos. Chem. Phys., 9, 8317–8330, https://doi.org/10.5194/acp-9-8317-2009, 2009.

Giglio, L., Justice, C., Boschetti, L., and Roy, D.: MCD64A1 MODIS/Terra+Aqua Burned Area Monthly L3 Global 500m SIN Grid V006 [Data set], NASA EOSDIS Land Processes DAAC [data set], https://doi.org/10.5067/MODIS/MCD64A1.006, 2015.

Giglio, L., Boschetti, L., Roy, D. P., Humber, M. L., and Justice, C. O.: The Collection 6 MODIS burned area mapping algorithm and product, Remote Sens. Environ., 217, 72–85, https://doi.org/10.1016/j.rse.2018.08.005, 2018.

Gilbert, M., Nicolas, G., Cinardi, G., Van Boeckel, T. P., Vanwambeke, S., Wint, W. G. R., and Robinson, T. P.: Global sheep distribution in 2010 (5 minutes of arc), Harvard Dataverse [data set], V3, https://doi.org/10.7910/DVN/BLWPZN, 2018a.

Gilbert, M., Nicolas, G., Cinardi, G., Van Boeckel, T. P., Vanwambeke, S., Wint, W. G. R., and Robinson, T. P.: Global pigs distribution in 2010 (5 minutes of arc), Harvard Dataverse [data set], V3, https://doi.org/10.7910/DVN/33N0JG, 2018b.

Gilbert, M., Nicolas, G., Cinardi, G., Van Boeckel, T. P., Vanwambeke, S., Wint, W. G. R., and Robinson, T. P.: Global goats distribution in 2010 (5 minutes of arc), Harvard Dataverse [data set], V3, https://doi.org/10.7910/DVN/OCPH42, 2018c.

Gilbert, M., Nicolas, G., Cinardi, G., Van Boeckel, T. P., Vanwambeke, S., Wint, W. G. R., and Robinson, T. P.: Global cattle distribution in 2010 (5 minutes of arc), Harvard Dataverse [data set], V3, https://doi.org/10.7910/DVN/GIVQ75, 2018d.

Gilbert, M., Nicolas, G., Cinardi, G., Van Boeckel, T. P., Vanwambeke, S., Wint, W. G. R., and Robinson, T. P.: Global chickens distribution in 2010 (5 minutes of arc), Harvard Dataverse [data set], V3, https://doi.org/10.7910/DVN/SUFASB, 2018e.

Gilbert, M., Nicolas, G., Cinardi, G., Van Boeckel, T. P., Vanwambeke, S., Wint, W. G. R., and Robinson, T. P.: Global buffaloes distribution in 2010 (5 minutes of arc), Harvard Dataverse [data set], V3, https://doi.org/10.7910/DVN/5U8MWI, 2018f.

Global Internal Displacement Monitoring Centre: Global Internal Displacement Database, available at: https://data.worldbank.org/indicator/VC.IDP.TOCV TS22 (last access: 20 June 2019), 2020.

Goode, J. G., Yokelson, R. J., Susott, R. A., and Ward, D. E.: Trace gas emissions from laboratory biomass fires measured by open-path Fourier transform infrared spectroscopy, J. Chem. Inf. Model., 104, 21237–21245, 1999.

Guo, X., Clarisse, L., Wang, R., Van Damme, M., Whitburn, S., Coheur, P., Clerbaux, C., Franco, B., Pan, D., Golston, L. M., Wendt, L., Sun, K., Tao, L., Miller, D., Mikoviny, T., Müller, M., Wisthaler, A., Tevlin, A. G., Murphy, J. G., Nowak, J. B., Roscioli, J. R., Volkamer, R., Kille, N., Neuman, J. A., Eilerman, S. J., Crawford, J. H., Yacovitch, T. I., Barrick, J. D., Scarino, A. J., and Zondlo, M. A.: Validation of IASI satellite ammonia observations at the pixel scale using in-situ vertical profiles, J. Geophys. Res.-Atmos., 126, e2020JD033475, https://doi.org/10.1029/2020jd033475, 2021.

Hazell, P. and Wood, S.: Drivers of change in global agriculture, Philos. Trans. R. Soc. Lond. B. Biol. Sci., 363, 495–515, https://doi.org/10.1098/rstb.2007.2166, 2008.

Hickman, J. E., Dammers, E., Galy-Lacaux, C., and van der Werf, G. R.: Satellite evidence of substantial rain-induced soil emissions of ammonia across the Sahel, Atmos. Chem. Phys., 18, 16713–16727, https://doi.org/10.5194/acp-18-16713-2018, 2018.

Hickman, J. E., Andela, N., Tsigaridis, K., Galy-Lacaux, C., Ossohou, M., and Bauer, S. E.: Reductions in NO_2 burden over north equatorial Africa from decline in biomass burning in spite of growing fossil fuel use, 2005 to 2017, P. Natl. Acad. Sci., 118, e2002579118, https://doi.org/10.1073/pnas.2002579118, 2021a.

Hickman, J. E., Dammers, E., Galy-Lacaux, C., Ossohou, M., and Bauer, S. E.: Continental and ecoregion-specific drivers of atmospheric NO_2 and NH_3 seasonality over Africa revealed by satellite observations, Global Biogeochem. Cy., 35, e2020GB006916, https://doi.org/10.1029/2020GB006916, 2021b.

Huffman, G. J., Adler, R. F., Bolvin, D. T., Gu, G., Nelkin, E. J., Bowman, K. P., Hong, Y., Stocker, E. F., and

Wolff, D. B.: The TRMM Multisatellite Precipitation Analysis (TMPA): Quasi-Global, Multiyear, Combined-Sensor Precipitation Estimates at Fine Scales, J. Hydrometeorol., 8, 38–55, https://doi.org/10.1175/jhm560.1, 2007.

Hurtmans, D., Coheur, P. F., Wespes, C., Clarisse, L., Scharf, O., Clerbaux, C., Hadji-Lazaro, J., George, M., and Turquety, S.: FORLI radiative transfer and retrieval code for IASI, J. Quant. Spectrosc. Radiat. Transf., 113, 1391–1408, https://doi.org/10.1016/j.jqsrt.2012.02.036, 2012.

Hurtmans, D., Clerbaux, C., and Coheur, P-F.: Daily IASI/Metop-A ULB-LATMOS carbon monoxide (CO) L2 product (total column), [data set], available at: https://iasi.aeris-data.fr/CO_IASI_A_data/ last access: February 2021. TS23

Idris, I.: Livestock and conflict in South Sudan – K4D Helpdesk Report 484, Institute of Development Studies, Brighton, 20 pp., 2018.

Kanter, D. R.: Nitrogen pollution: a key building block for addressing climate change, Climatic Change, 147, 11–21, https://doi.org/10.1007/s10584-017-2126-6, 2018.

Kerzenmacher, T., Dils, B., Kumps, N., Blumenstock, T., Clerbaux, C., Coheur, P.-F., Demoulin, P., García, O., George, M., Griffith, D. W. T., Hase, F., Hadji-Lazaro, J., Hurtmans, D., Jones, N., Mahieu, E., Notholt, J., Paton-Walsh, C., Raffalski, U., Ridder, T., Schneider, M., Servais, C., and De Mazière, M.: Validation of IASI FORLI carbon monoxide retrievals using FTIR data from NDACC, Atmos. Meas. Tech., 5, 2751–2761, https://doi.org/10.5194/amt-5-2751-2012, 2012.

Korontzi, S., McCarty, J., Loboda, T., Kumar, S., and Justice, C.: Global distribution of agricultural fires in croplands from 3 years of Moderate Resolution Imaging Spectroradiometer (MODIS) data, Global Biogeochem. Cy., 20, GB2021, https://doi.org/10.1029/2005GB002529, 2006.

Krupa, S. V.: Effects of atmospheric ammonia (NH_3) on terrestrial vegetation: A review, Environ. Pollut., 124, 179–221, https://doi.org/10.1016/S0269-7491(02)00434-7, 2003.

Lee, C., Martin, R. V., Van Donkelaar, A., Lee, H., Dickerson, R. R., Hains, J. C., Krotkov, N., Richter, A., Vinnikov, K., and Schwab, J. J.: SO_2 emissions and lifetimes: Estimates from inverse modeling using in situ and global, space-based (SCIAMACHY and OMI) observations, J. Geophys. Res.-Atmos., 116, D06304, https://doi.org/10.1029/2010JD014758, 2011.

Lelieveld, J., Evans, J. S., Fnais, M., Giannadaki, D., and Pozzer, A.: The contribution of outdoor air pollution sources to premature mortality on a global scale, Nature, 525, 367–371, https://doi.org/10.1038/nature15371, 2015.

Masso, C., Nziguheba, G., Mtutegi, J., Galy-Lacaux, C., Wendt, K., Butterbach-Bahl, K., Wairegi, L., and Datta, A.: Soil fertility Managment in Sub-Saharan Africa, in Sustainable Agriculture Reviews, edited by: Lichtfouse, E., Springer International Publishing, Cham,, 205–231, 2017.

Matson, P. A., McDowell, W. H., Townsend, A. R., and Vitousek, P. M.: The globalization of N deposition: ecosystemconsequences in tropical environments, Biogeochemistry, 46, 67–83, 1999.

Nicholson, S., Some, B., McCollum, J., Nelkin, E., Klotter, D., Berte, Y., Diallo, B., Gaye, I., Kpabeba, G., Ndiaye, O., Noukpozounkou, J., Tanu, M., Thiam, A., Toure, A., and Traore, A.: Validation of TRMM and other rainfall estimates with a high-density gauge dataset for West Africa. Part II: Validation of TRMM rainfall products, J. Appl. Meteorol., 42, 1355–1368, 2003.

Ossohou, M., Galy-Lacaux, C., Yoboué, V., Hickman, J. E., Gardrat, E., Adon, M., Darras, S., Laouali, D., Akpo, A., Ouafo, M., Diop, B., and Opepa, C.: Trends and seasonal variability of atmospheric NO_2 and HNO_3 concentrations across three major African biomes inferred from long-term series of ground-based and satellite measurements, Atmos. Environ., 207, 148–166, 2019.

Pommier, M., Law, K. S., Clerbaux, C., Turquety, S., Hurtmans, D., Hadji-Lazaro, J., Coheur, P.-F., Schlager, H., Ancellet, G., Paris, J.-D., Nédélec, P., Diskin, G. S., Podolske, J. R., Holloway, J. S., and Bernath, P.: IASI carbon monoxide validation over the Arctic during POLARCAT spring and summer campaigns, Atmos. Chem. Phys., 10, 10655–10678, https://doi.org/10.5194/acp-10-10655-2010, 2010.

Pope, C. A., Burnett, R. T., Thun, M. J., Calle, E. E., Krewski, D., Ito, K., and Thurston, G. D.: Long-term Exposure to Fine Particulate Air Pollution, J. Am. Med. Assoc., 287, 1132–1141, https://doi.org/10.1001/jama.287.9.1132, 2002.

Raleigh, C., Linke, A., Hegre, H., and Karlsen, J.: Introducing ACLED: An Armed Conflict Location and Event Dataset: Special Data Feature, J. Peace Res., 47, 651–660, https://doi.org/10.1177/0022343310378914, 2010.

Ramo, R., Roteta, E., Bistinas, I., van Wees, D., Bastarrika, A., Chuvieco, E., and van der Werf, G. R.: African burned area and fire carbon emissions are strongly impacted by small fires undetected by coarse resolution satellite data, P. Natl. Acad. Sci., 118, e2011160118, https://doi.org/10.1073/pnas.2011160118, 2021.

Robinson, T. P., Wint, G. R. W., Conchedda, G., Van Boeckel, T. P., Ercoli, V., Palamara, E., Cinardi, G., D'Aietti, L., Hay, S. I., and Gilbert, M.: Mapping the Global Distribution of Livestock, PLoS One, 9, e96084, https://doi.org/10.1371/journal.pone.0096084, 2014.

Rose, A., McKee, J. J., Urban, M. L., and Bright, E. A.: LandScan 2017, Oak Ridge National Laboratory [data set], available at: https://landscan.ornl.gov/downloads/2017 (last access: 29 June 2019), 2018. TS24

Roteta, E., Bastarrika, A., Padilla, M., Storm, T., and Chuvieco, E.: Development of a Sentinel-2 burned area algorithm: Generation of a small fire database for sub-Saharan Africa, Remote Sens. Environ., 222, 1–17, https://doi.org/10.1016/j.rse.2018.12.011, 2019.

Rufino, M. C., Rowe, E. C., Delve, R. J., and Giller, K. E.: Nitrogen cycling efficiencies through resource-poor African crop-livestock systems, Agric. Ecosyst. Environ., 112, 261–282, https://doi.org/10.1016/j.agee.2005.08.028, 2006.

Sauvage, B., Gheusi, F., Thouret, V., Cammas, J.-P., Duron, J., Escobar, J., Mari, C., Mascart, P., and Pont, V.: Medium-range midtropospheric transport of ozone and precursors over Africa: two numerical case studies in dry and wet seasons, Atmos. Chem. Phys., 7, 5357–5370, https://doi.org/10.5194/acp-7-5357-2007, 2007.

Stevens, C. J., David, T. I., and Storkey, J.: Atmospheric nitrogen deposition in terrestrial ecosystems: Its impact on plant communities and consequences across trophic levels, Funct. Ecol., 32, 1757–1769, https://doi.org/10.1111/1365-2435.13063, 2018.

Sutton, M. A., Reis, S., Riddick, S. N., Dragosits, U., Nemitz, E., Theobald, M. R., Tang, Y. S., Braban, C. F., Vieno, M., Dore, A. J., Mitchell, R. F., Wanless, S., Daunt, F., Fowler, D., Blackall, T. D., Milford, C., Flechard, C. R., Loubet, B.,

Massad, R., Cellier, P., Personne, E., Coheur, P. F., Clarisse, L., Van Damme, M., Ngadi, Y., Clerbaux, C., Skøth, C. A., Geels, C., Hertel, O., Wichink Kruit, R. J., Pinder, R. W., Bash, J. O., Walker, J. T., Simpson, D., Horváth, L., Misselbrook, T. H., Bleeker, A., Dentener, F., and de Vries, W.: Towards a climate-dependent paradigm of ammonia emission and deposition, Philos. Trans. R. Soc. B Biol. Sci., 368, 20130166, https://doi.org/10.1098/rstb.2013.0166, 2013.

Tian, D. and Niu, S.: A global analysis of soil acidification caused by nitrogen addition, Environ. Res. Lett., 10, 024019, https://doi.org/10.1088/1748-9326/10/2/024019, 2015.

Tropical Rainfall Measuring Mission (TRMM): TRMM (TMPA/3B43) Rainfall Estimate L3 1 month 0.25 degree x 0.25 degree V7, Greenbelt, MD, Goddard Earth Sciences Data and Information [data set], https://doi.org/10.5067/TRMM/TMPA/MONTH/7, 2011. `TS25`

United Nations High Commissioner on Refugees: Refugee Data Finder, [data set], available at: https://data.worldbank.org/indicator/VC.IDP.NWCV, 2020. `TS26`

USDA Agricultural Air Quality Task Force: Ammonia Emissions: What To Know Before You Regulate, Washington, DC, available at: http://www.nrcs.usda.gov/wps/portal/nrcs/detail/national/air/taskforce/?cid=stelprdb1268645 (last access: 29 June 2020), 9 pp., 2014.

Van Damme, M., Wichink Kruit, R. J., Schaap, M., Clarisse, L., Clerbaux, C., Coheur, P. F., Dammers, E., Dolman, A. J., and Erisman, J. W.: Evaluating 4 years of atmospheric ammonia (NH_3) over Europe using IASI satellite observations and LOTOS-EUROS model results, J. Geophys. Res., 119, 9549–9566, https://doi.org/10.1002/2014JD021911, 2014a.

Van Damme, M., Clarisse, L., Heald, C. L., Hurtmans, D., Ngadi, Y., Clerbaux, C., Dolman, A. J., Erisman, J. W., and Coheur, P. F.: Global distributions, time series and error characterization of atmospheric ammonia (NH_3) from IASI satellite observations, Atmos. Chem. Phys., 14, 2905–2922, https://doi.org/10.5194/acp-14-2905-2014, 2014b.

Van Damme, M., Clarisse, L., Dammers, E., Liu, X., Nowak, J. B., Clerbaux, C., Flechard, C. R., Galy-Lacaux, C., Xu, W., Neuman, J. A., Tang, Y. S., Sutton, M. A., Erisman, J. W., and Coheur, P. F.: Towards validation of ammonia (NH_3) measurements from the IASI satellite, Atmos. Meas. Tech., 8, 1575–1591, https://doi.org/10.5194/amt-8-1575-2015, 2015.

Van Damme, M., Whitburn, S., Clarisse, L., Clerbaux, C., Hurtmans, D., and Coheur, P.-F.: Version 2 of the IASI NH_3 neural network retrieval algorithm: near-real-time and reanalysed datasets, Atmos. Meas. Tech., 10, 4905–4914, https://doi.org/10.5194/amt-10-4905-2017, 2017.

Van Damme, M., Clarisse, L., Whitburn, S., Hadji-Lazaro, J., Hurtmans, D., Clerbaux, C., and Coheur, P.: Industrial and agricultural ammonia point sources exposed, Nature, 564, 99–103, 2018.

Van Damme, M., Clarisse, L., Franco, B., Sutton, M. A., Erisman, J. W., Wichink Kruit, R., van Zanten, M., Whitburn, S., Hadji-Lazaro, J., Hurtmans, D., Clerbaux, C., and Coheur, P.-F.: Global, regional and national trends of atmospheric ammonia derived from a decadal (2008–2018) satellite record, Environ. Res. Lett., 16, 055017, https://doi.org/10.1088/1748-9326/abd5e0, 2021.

van der A, R. J., Eskes, H. J., Boersma, K. F., van Noije, T. P. C., Van Roozendael, M., De Smedt, I., Peters, D. H. M. U., and Meijer, E. W.: Trends, seasonal variability and dominant NO_x source derived from a ten year record of NO_2 measured from space, J. Geophys. Res.-Atmos., 113, D04302, https://doi.org/10.1029/2007JD009021, 2008.

Vitousek, P., Naylor, R., Crews, T., David, M., Drinkwater, L., Holland, E., Johnes, P., Katzenberger, J., Martinelli, L. A., Matson, P. A., Nziguheba, G., Ojima, D., Palm, C. A., Robertson, G., Sanchez, P., Townsend, A., and Zhang, F.: Nutrient Imbalances in Agricultural Development, Science, 324, 1519–1520, 2009.

Vrieling, A., de Beurs, K. M., and Brown, M. E.: Variability of African farming systems from phenological analysis of NDVI time series, Climatic Change, 109, 455–477, https://doi.org/10.1007/s10584-011-0049-1, 2011.

Warner, J. X., Dickerson, R. R., Wei, Z., Strow, L. L., Wang, Y., and Liang, Q.: Increased atmospheric ammonia over the world's major agricultural areas detected from space, Geophys. Res. Lett., 44, 2875–2884, https://doi.org/10.1002/2016GL072305, 2017.

Whitburn, S., Van Damme, M., Kaiser, J. W., Van Der Werf, G. R., Turquety, S., Hurtmans, D., Clarisse, L., Clerbaux, C., and Coheur, P. F.: Ammonia emissions in tropical biomass burning regions: Comparison between satellite-derived emissions and bottom-up fire inventories, Atmos. Environ., 121, 42–54, https://doi.org/10.1016/j.atmosenv.2015.03.015, 2015.

World Bank: World Bank Open Data, World Bank Open Data, available at: https://data.worldbank.org/indicator/SM.POP.REFG.OR `TS27`, last access: 2 February 2019.

Yegbemey, R. N., Kabir, H., Awoye, O. H. R., Yabi, J. A., and Paraïso, A. A.: Managing the agricultural calendar as coping mechanism to climate variability: A case study of maize farming in northern Benin, West Africa, Clim. Risk Manag., 3, 13–23, https://doi.org/10.1016/j.crm.2014.04.001, 2014.

Yokelson, R. J., Christian, T. J., Karl, T. G., and Guenther, A.: The tropical forest and fire emissions experiment: laboratory fire measurements and synthesis of campaign, Rev. Int. Acupunct., 8, 3509–3527, https://doi.org/10.1016/s1887-8369(09)71579-0, 2008.

Zhang, H.-M., Huang, B., Lawrimore, J., Menne, M., Smith, T. M.: NOAA Global Surface Temperature Dataset (NOAAGlobalTemp), Version 5, NOAA National Centers for Environmental Information [data set], https://doi.org/10.25921/9qth-2p70, 2021. `TS28`

Zheng, B., Chevallier, F., Ciais, P., Yin, Y., and Wang, Y.: On the Role of the Flaming to Smoldering Transition in the Seasonal Cycle of African Fire Emissions, Geophys. Res. Lett., 45, 11998-12007, https://doi.org/10.1029/2018GL079092, 2018.

Remarks from the typesetter